ISSN 1070-3284, Russian Journal of Coordination Chemistry, 2018, Vol. 44, No. 5, pp. 322–334. © Pleiades Publishing, Ltd., 2018.

Crystal Structures, Cytotoxicity, Cell Apoptosis Mechanism, and DNA Binding of Two 8-Hydroxylquinoline Zinc(II) Complexes[1]

H. R. Zhang[a, b, *], Y. C. Liu[c], Z. F. Chen[c], J. Guo[a], Y. X. Peng[a], and H. Liang[c]

[a] *College of Materials and Environmental Engineering, Hunan University of Humanities, Science and Technology, Loudi, Hunan, 417000 P.R. China*

[b] *College of Chemistry and Chemical Engineering, Central South University, Changsha, Hunan, 410083 P.R. China*

[c] *State Key Laboratory for the Chemistry and Molecular Engineering of Medicinal Resources, School of Chemistry and Pharmacy of Guangxi Normal University, Guilin, 541004 P.R. China*

**e-mail: zhr328@163.com*

Received June 23, 2017

Abstract—Two zinc(II) complexes, $[Zn_4(HOQ)_6Ac_2]$ (**I**) (HOQ = 8-hydroxylquinoline) and $[Zn_4(MeQ)_6Ac_2]$ (**II**) (MeQ = 2-methyl-8-hydroxylquinoline), were synthesized and characterized by IR spectroscopy, ESI-MS spectrometry, elemental analysis and single crystal X-ray diffraction analysis (CIF files CCDC nos. 1433544 (**I**) and 1433546 (**II**)). The in vitro cytotoxicity of the two complexes, which was first reported, was evaluated by MTT assay against a series of tumor cell lines as well as HL-7702 normal liver cell line. The results indicated that they showed significantly higher cytotoxicity than cispltain on BEL-7404 cells with IC_{50} values of 11.85 ± 0.06 μM (**I**) and 8.40 ± 0.07 μM (**II**), respectively. Further apoptosis mechanism studies on BEL-7404 cells suggested that their antitumor activities were achieved through cell apoptosis and arrest at G1 or S phase. The decline of mitochondrial membrane potential, the elevation of reactive oxygen species and cytoplasmic calcium concentration ($[Ca^{2+}]_c$), the raise of caspase-3/9 activity indicated that complexes **I** and **II** induced apoptosis of BEL-7404 by a mitochondrial dysfunction pathway. Investigations on the binding properties of complexes **I** and **II** to ct-DNA by UV-Vis, circular dichroism spectra and agarose gel electrophoresis indicated that the two complexes could bind with ct-DNA via an intercalative mode.

Keywords: 8-hydroxylquinoline, 2-methyl-8-hydroxylquinoline, zinc(II) complex, cytotoxicity, cell apoptosis, DNA binding

DOI: 10.1134/S107032841805007X

INTRODUCTION

Nowadays, cancer is one of the leading threats to human health [1]. It is the second largest cause of death in the world after cardiovascular disease. Therefore, the research and development of low toxicity, effective novel anti-tumor drugs have caused many medical, biological and chemical researchers' close attentions [2–6]. Since the discovery of cisplatin and its derivatives as potential anticancer agents [7], platinum-based compounds have gained much attention for anticancer agents [8]. But because of the serous side effects of cisplatin and related platinum complexes, including nephrotoxicity, emetogenesis and neurotoxicity [9]. Therefore, there is an increasing need for the development of other anticancer transition metal complexes with better anticancer activity [10].

Zinc, which is the second most abundant transition metal in organisms after iron, is one of essential trace elements in human body [11]. It plays a very important role in human growth and development, reproductive and genetic, immune, endocrine and other important biological process. For example, zinc is involved in many physiological processes such as DNA and protein synthesis, where zinc acts as a cofactor for proteins and plays a very important role as a signaling molecule in synaptic plasticity [12]. In addition, many research reports suggest that zinc complexes have rapid ligand exchange property and lower toxicity as potential anticancer agent [13, 14].

On the other hand, quinoline and its derivatives had been attracting special attention of medicinal chemistry researchers in recent years due to their therapeutic properties. A series of quinoline derivatives had been reported to possess potential anticancer activities [15]. It was well known that quinoline sulphonamides had been used in the treatment of cancer, tuberculosis, diabetes, malaria, and convulsion [16]. Over the past seven years, Lam et al. reported the antitumor activities of quinoline type compounds. In par-

[1] The article is published in the original.

ticular, they found out that 8-hydroxyquinoline derivatives are effective for anti-tumor agents [17–19].

In view of developing new Zn(II) anti-tumor agents, in this work, we synthesized two kind of zinc complexes with 8-hydroxylquinoline (HOQ) and 2-methyl-8-hydroxylquinoline (MeQ), studied their cytotoxicity in vitro against seven selected tumor cell lines, proposed a possible anti-tumor mechanism, and investigated their binding properties to DNA by means of UV-Vis, circular dichroism (CD) spectroscopy, agarose gel electrophoresis assay.

EXPERIMENTAL

Materials and methods. All the chemical reagents were commercially available (analytical grade) and used without purification. HOQ and MeQ were purchased from Alfa-aesar. RPMI 1640 and fetal bovine serum (FBS) were obtained from Hyclone (USA). 3-(4,5-Dimathylthiazol-2-yl)-2,5-diphenyltetrazolium bromide (MTT), Hoechst 33258, RNase A, Propidium iodide (PI), JC-1, and Acridine orange/Ethidium bromide (AO/EB), 2',7'-dichlorofluorescein-diacetate (DCFH-DA), Fluo-3 AM were purchased from Sigma Chemicals Co. (USA). The CasPGLOW™ Fluorescein Activite Caspase-3 and Caspase-9 Staining kit were obtained from BioVision. Calf thymus DNA (ct-DNA) was purchased from Sigma. PBR322 DNA was purchased from Thermo Scientific (USA). Tris-HCl-NaCl buffer (TSB, 5 mM Tris, 50 mM NaCl, pH 7.40) was prepared in two times distilled water. All solvent used for spectroscopic studies were HPLC grade.

Infrared spectra were carried out as KBr pellets on a PerkineElmer FT-IR Spectrometer. Elemental analyses (C, H, N) were obtained by Perkin Elmer Series II CHNS/O 2400 elemental analyzer. ESI-MS (electrospray ionization mass spectrum) were recorded on a Bruker HCT Electrospray Ionization Mass Spectrometer. Flow Cytometry (FCM) was recorded on FACS AriaII Flow Cytometer (BD Biosciences, San Jose, USA). UV-Vis absorption spectra were recorded on a Perkin-Elmer Lambda45 UV-Visible spectrophotometer. CD spectra of ct-DNA were performed on from a JASCOJ-810 automatic recording spectropolarimeter.

Synthesis of complex I. $Zn(OAc)_2 \cdot H_2O$ (0.1 mmol, 0.017 g), HOQ (0.1 mmol, 0.015 g), methanol (0.6 mL) and chloroform (0.1 mL) were placed in a thick Pyrex tube (~25 cm long), then the mixture was frozen by liquid N_2, evacuated under vacuum, sealed and reacted at 110°C for three days. Received yellow block crystals of complex **I** were used for X-ray diffraction analysis. The yield was 0.018 g (86%).

ESI-MS (DMSO; *m/z*): 1134.4 $[Zn_4(OQ)_6 + H_2O]^{2+}$. IR (KBr; ν, cm^{-1}): 3431 m ν(OH), 1579 s ν(C=N), 1466 s ν(C=C), 1272 s ν(C–N), 1109 s ν(C–O), 599 s ν(Zn–N), 501 s ν(Zn–O).

For $C_{58}H_{42}N_6O_{10}Zn_4$			
Anal. calcd., %	C 55.97	H 3.40	N 6.75
Found, %	C 55.07	H 3.81	N 6.61

Synthesis of complex II was carried out with the same processing step for complex **I** using MeQ instead HOQ. Yellow crystals of complex **II** were generated after three days, choose suitable crystals for X-ray analysis. The yield was 0.018 g (82%).

ESI-MS (DMSO; *m/z*): 1368 $[Zn_4(MeQ)_6 + H_2O]^{2+}$. IR (KBr; ν, cm^{-1}): 3373 m ν(OH), 2931 w ν(C–H), 1574 s ν(C=N), 1461 s ν(C=C), 1278 s ν(C–N), 1111 s ν(C–O), 528 s ν(Zn–N), 409 s ν(Zn–O).

For $C_{64}H_{54}N_6O_{10}Zn_4$			
Anal. calcd., %	C 57.85	H 4.10	N 6.32
Found, %	C 57.83	H 4.27	N 6.29

X-ray crystallography. The single-crystal X-ray diffraction date for the complexes **I** and **II** were collected at room temperature on a Bruker Smart Apex II CCD diffractometer equipped with graphite monochromated MoK_α radiation (λ = 0.71073 Å). The structure was solved with direct methods and refined using SHELXL-97 programs [20]. The non-hydrogen atoms were refined anisotropically by full-matrix least squares methods. All hydrogen atoms were placed geometrically and the positional parameters were refined using a riding model. The images of the complexes were created with the DIAMOND program [21]. The detailed crystallographic data and structural refinement parameters are summarized in Table 1. Selected bond distances and angles are listed in Table 2.

Supplementary material for structures has been deposited with the Cambridge Crystallographic Data Centre (CCDC nos. 1433544 (**I**) and 1433546 (**II**); deposit@ccdc.cam.ac.uk or http://www.ccdc.cam.ac.uk).

Cytotoxicity assay in vitro. The BEL-7404, HeLa, HepG2, MGC-803, SK-OV-3, T-24 tumor cell lines and HL-7702 human normal liver cell were purchased from the Shanghai Cell Bank of the Chinese Academy of Sciences. The cell lines were located in DMEN (Gibco, Scotland, UK) at 37°C in a humidified atmosphere of 5% CO_2/95% air and cultured in RPMI-1640 medium supplemented with 10% FBS, 100 units/mL penicillin and 100 μg/mL streptomycin. Cisplatin was selected as a reference metallodrug for investigating the potency of these synthetic complexes [22].

Assays of cytotoxicity were carried out in 96-well, flat bottomed microtitre plates. 180 μL supplemented

Table 1. Crystallographic data and structure refinement for complexes **I** and **II**

Parameter	Value	
	I	**II**
Formula weight	1244.55	1328.70
Temperature, K	293(2)	293(2)
Crystal system	Triclinic	Triclinic
Space group	$P\bar{1}$	$P\bar{1}$
a, Å	11.4134(7)	11.5790(13)
b, Å	11.9211(9)	11.8780(12)
c, Å	11.9973(8)	12.5446(15)
α, deg	102.853(6)	116.842(11)
β, deg	103.052(6)	106.461(10)
γ, deg	112.081(6)	96.023(9)
V, Å^3	1385.51(17)	1420.6(3)
Z	2	2
ρ_{calcd}, mg mm^{-3}	1.535	1.553
μ, m^{-1}	1.779	1.735
F(000)	652	680
Crystal size, mm	0.44 × 0.20 × 0.15	0.25 × 0.20 × 0.15
2θ Range for data collection, deg	6.24–52.74	5.74–52.74
Index ranges	$-14 \le h \le 14$, $-14 \le k \le 14$, $-14 \le l \le 14$	$-14 \le h \le 14$, $-13 \le k \le 14$, $-15 \le l \le 15$
Reflections collected	14723	14554
Independent reflections (R_{int})	5654 (0.0383)	5763 (0.0720)
Data/restraints/parameters	5654/3/368	5763/0/383
Goodness-of-fit on F^2	1.044	1.045
Final R indexes ($I > 2\sigma(I)$)	$R_1 = 0.0382$, $wR_2 = 0.0792$	$R_1 = 0.0846$, $wR_2 = 0.1843$
Final R indexes (all data)	$R_1 = 0.0587$, $wR_2 = 0.0888$	$R_1 = 0.1376$, $wR_2 = 0.2129$
Largest diff. peak and hole, e Å^{-3}	0.385/–0.338	1.420/–0.503

culture medium with a density of 1×10^4 cells per well was added to each well and the cells allowed to attach overnight. Complexes **I** and **II**, cisplatin were added in the culture medium with 1% DMSO to give various concentrations (2.5, 5, 10, 20, 40 μM, respectively). The microtitre plates were incubated at 37°C in a humidified atmosphere of 5% CO_2/95% air for further 48 h. At the end of each incubation period, 10 μL of 5 mg/mL MTT solution in phosphate buffered saline (PBS, pH 7.40) was added into each well and the cultures were incubated further for 4 h. After pouring out the supernatant, 100 μL of DMSO was added to dissolve the formazan crystals. The absorbance was recorded by enzyme labeling instrument with 490/630 nm double wavelength measurement. The cytotoxicity was evaluated according to the percentage of cell survival in a dose-dependent manner relative to the negative control. The IC_{50} values were calculated by the Bliss method ($n = 5$). All the tests were repeated in at least three independent trials.

Cell cycle assay. BEL-7404 cells treated with different concentrations of synthetic complexes **I** and **II** at 0, 5.0, 10.0, 15.0 μM for 48 h were harvested, centrifuged, washed with ice-cold PBS, fixed in 75% ethanol and stored at –20°C overnight. The fixed cells were stained with 0.5 mL of PBS containing 50 μg/mL PI in the presence of 100 μg/mL RNaseA for 45 min at 37°C in the dark. Cell cycle profile was analyzed by FACS AriaII flow cytometer.

Cell apoptosis assay. After chemical treatment with different concentrations (0, 5.0, 10.0, 15.0 μM) of the complexes **I** and **II** for 8 h, BEL-7404 cells were collected, washed with PBS, added 100 μL 1× binding buffer, 5 μL of annexin V-FITC and 5 μL of PI, main-

Table 2. Selected bond lengths (Å) and angles (deg) for complexes **I** and **II**

Bond	*d*, Å	Bond	*d*, Å	Bond	*d*, Å
		I			
Zn(1)–O(1)	2.0814(18)	Zn(1)–N(1)	2.105(2)	Zn(2)–O(3)	2.2593(18)
Zn(1)–O(2)	2.0711(19)	Zn(1)–N(2)	2.103(2)	Zn(2)–O(4)	2.009(2)
Zn(1)–O(3)	2.1861(18)	Zn(2)–O(1)	2.0065(19)	Zn(2)–N(3)	2.093(2)
		II			
Zn(1)–O(1)	2.013(5)	Zn(1)–O(4)	2.007(6)	Zn(2)–O(1)	2.008(5)
Zn(1)–O(2)	2.054(5)	Zn(1)–N(2)	2.158(7)	Zn(2)–N(1)	2.085(6)
Angle	ω, deg	Angle	ω, deg	Angle	ω, deg
		I			
O(1)Zn(1)O(3)	79.42(7)	O(2)Zn(1)N(2)	78.75(9)	O(1)Zn(2)N(3)	100.68(9)
O(1)Zn(1)N(1)	79.15(8)	N(1)Zn(1)O(3)	156.03(8)	O(4)Zn(2)O(3)	171.02(7)
O(1)Zn(1)N(2)	100.50(9)	N(2)Zn(1)O(3)	96.46(8)	O(4)Zn(2)N(3)	97.48(9)
O(2)Zn(1)O(1)	173.19(7)	N(2)Zn(1)N(1)	97.89(9)	N(3)Zn(2)O(3)	75.55(8)
O(2)Zn(1)O(3)	93.90(7)	O(1)Zn(2)O(3)	79.26(7)	Zn(2)O(1)Zn(1)	106.09(8)
O(2)Zn(1)N(1)	107.66(9)	O(1)Zn(2)O(4)	107.93(8)	Zn(1)O(3)Zn(2)	94.59(7)
		II			
O(1)Zn(2)N(3)	100.68(9)	O(4)Zn(1)O(1)	113.2(2)	O(4)Zn(1)N(2)	101.9(3)
O(1)Zn(1)N(2)	96.8(2)	O(4)Zn(1)O(1)	157.1(3)	O(1)Zn(2)N(2)	81.3(2)

tained at 4°C for 20 min in the dark, and finally resuspended in 400 μL 1× binding buffer. Then the stained cells were tested by flow cytometry within an hour.

Live cell fluorescence microscopy. (1) Hoechst 33258 staining assay. BEL-7404 cells were cultured in 6-well tissue culture plates with a coverslip and treated with 0, 5.0, 10.0, 15.0 μM complexes **I** and **II** for further 8 h after the cells adhered. Then, treated cells were fixed by 0.5 mL of stationary liquid for 10 min, washed twice with PBS, stained with 0.5 mL Hoechst 33258 for 5 min, washed with PBS again. Finally, dropped a blob of anti-fluorescence quenching liquid on slide, covered by coverslip, making cells contact anti-fluorescence quenching liquid enough without bubbles. Changes in nuclear morphology were detected by a Zeiss LSM710 confocal microscope.

(2) AO/EB staining assay. To determine the presence of apoptotic cells, BEL-7404 cells were cultured and treated with the same processing step for Hoechst 33258 staining assay, the treated and control BEL-7404 cells were stained with AO and EB together. Each of the following four cellular states was recorded: (i) live cells with normal nuclei, bright green chromatin and organized structure; (ii) apoptotic cells with highly condensed or fragmented bright green-yellow chromatin; (iii) dead cells with normal nuclei, bright red chromatin and organized structure; and (iv) dead cells with apoptotic nuclei, bright orange chromatin, which were highly condensed and fragmented [23, 24].

Measurement of mitochondrial membrane potential. The loss of mitochondria membrane potential ($\Delta\Psi$) was evaluated by using a fluorescent dye 3,6-diamino-9-[2-(methoxycarbonyl)phenyl]xanthylium chloride (Rhodamine (Rh) 123). BEL-7404 cells were seeded in 6-well plates and treated with 10.0 μM of complexes **I** and **II** for 8 h. Then, treated and control BEL-7404 cells were harvested, washed with PBS, stained with 10 μg/mL Rh 123 for 30 min at 37°C, centrifuged, washed with culture medium, and tested by flow cytometry immediately.

Measurement of ROS production. Intracellular ROS level was measured using the stain of DCFH-DA oxidation by flow cytometry. BEL-7404 cells were treated with 10.0 μM of complexes **I** and **II** for 8 h at 37°C, collected and washed with PBS. After DCFH-DA (100 μM) incubation for 30 min in the dark at 37°C, cells were washed thrice with serum-free cell culture medium and immediately analyzed.

Measurement of cytoplasmic calcium concentration ($[Ca^{2+}]_c$). Intracellular Ca^{2+} concentration was measured in by flow cytometry with Fluo-3 acetoxymethyl ester (Fluo-3 AM). BEL-7404 cells were treated with 10.0 μM of complexes **I** and **II**, stained with 5 μM Fluo-3 AM for 30 min at 37°C in the dark, washed with PBS thrice, and tested immediately using flow cytometry.

Determination of caspase-3 and caspase-9 activity by flow cytometric analysis. Caspase-3 and caspase-9 activity were assessed using FITC-DEVD-FMK (for caspase-3) or FITC-LEHD-FMK (for caspase-9) by flow cytometric. BEL-7404 cells treated with 10.0 μM

of complexes **I** and **II** for 8 h were collected, centrifuged, washed with PBS thrice, added 300 μL buffer, and then 1 μL caspase-3 substrate (FITC-DEVD-FMK) and caspase-9 substrate (FITC-LEHD-FMK) were added, incubated at 37°C for 1 h. Cells were tested by a FACS AriaII flow cytometer equipped with a 488 nm argon laser. The analysis results were represented as the percent change on the activity comparing with the untreated control.

DNA-binding studies. (1) Spectroscopic studies on DNA interaction. The stock solution of ct-DNA (2.0×10^{-3} M) was stored at 4°C for no more than 5 days before use. The synthesized complexes **I** and **II** were all prepared as 2.0×10^{-3} M DMSO stock solutions for DNA binding studies. The final working solutions of the complexes for DNA binding studies were diluted by TSB (DMSO containing was less than 10%). For electrostatic interaction experiments, the 3.0 mL working solution containing 2.0×10^{-5} M complexes was titrated by successive additions of sodium dodecyl sulfonate (SDS) solution. After each addition, the mixed solution was allowed to incubate for 5 min before the the absorption intensity was measured. For UV-Vis absorption experiments, the working solutions of the complexes were constantly adding ct-DNA stock solution and then tested after incubating for 5 min. K_b as the equilibrium DNA binding constant was calculated according to the Wolfe–Shimer equation [25]:

$$\frac{[DNA]}{(\varepsilon_a - \varepsilon_f)} = \frac{[DNA]}{(\varepsilon_b - \varepsilon_f)} + \frac{1}{K_b(\varepsilon_b - \varepsilon_f)}, \quad (1)$$

where [DNA] is the concentration of DNA in nucleotides and ε_a is the observed extinction coefficient ($A_{obsd}/[M]$), ε_f and ε_b are the extinction coefficient of the free compound and the extinction coefficient of the compound in the fully DNA-bound form, respectively. The CD spectra was measured over 200–400 nm at 100 nm/min, DNA (1.0×10^{-4} M) was added each complex (4.0×10^{-4} M). The added complexes were incubated with DNA for 10 min before recording. The background CD signal of TSB was subtracted in advance.

(2) Agarose gel electrophoretic assay. In agarose gel electrophoretic experiments, the DMSO stock solution of all complexes were diluted to gradient concentrations of 10, 20, 40, 60, 80, 100 μM by TBE buffer (TBE = Tris-Boric acid–EDTA buffer solution). The diluted solution of each complexes were mixed with 0.5 μg DNA (pBR322 DNA) and brought to 25 μL by TBE buffer. All samples were incubated at 37°C in dark for 2 h, and 2 mL DNA loading buffer was added to every 18 μL of each sample, and the mixture was electrophoresed through 1% agarose gel that immersed in the TBE buffer for 4 h at 70 V electric field. Then the gel was immersed in EB (1 μg/mL) solution for 30 min. The DNA bands were visualized by placing the gel on UV illuminator and photographed.

Statistical analysis. The data processing was treated using SPSS 17.0 software taking $P < 0.05$ as statistically significant.

RESULTS AND DISCUSSION

The single-crystal X-ray diffraction analyses for complexes **I** and **II** revealed that their structures are similar. The structures of complexes **I** and **II** with labeled atoms are shown in Fig. 1. For complex **I**, the single-crystal structure is consistent with the reported literature [26]. The Zn(1) atom chelated by two 8-hydroxylquinoline anions is six coordinate in a four double tapered angle coordination geometry, while the Zn(2) atom, which is chelated by a 8-hydroxylquinoline anion and an acetate anion, is five coordinate in a square-pyramidal coordination geometry. For complex **II**, compared with complex **I**, in addition to the ligand (8-hydroxyquinoline is replaced by 2-methyl-8-hydroxyquinoline), the other are the same.

Complexes **I** and **II** were tested for their stabilities in the physiological conditions (TSB buffer solution with pH value of 7.40, containing 1% DMSO) by UV-Vis spectroscopy. As shown in Fig. 2, the time-dependent (in the time course of 0, 1, 24, 48 h) UV-Vis spectra for both of complexes displayed no obvious changes in the spectral characteristics over time, which indicated that the complexes' coordination mode of the corresponding 8-hydroxyquinoline ligand to the metal centre was not changed and both of complexes were stable in TSB buffer solution for 48 h at room temperature.

The cytotoxicities of complexes **I** and **II** against SK-OV-3, BEL-7404, HepG2, HeLa, T-24, MGC-803 cells were estimated by MTT assay, and their toxicities to normal cells were also evaluated using the HL-7702 cells. Their in vitro antitumor activities were quantified by determining the corresponding IC_{50} values. As shown in Table 3, the IC_{50} values of complexes **I** and **II** against BEL-7404 cells were the lowest among the six selected tumor cell lines, displaying high cytotoxicity against BEL-7404 cells. Comparing with cisplatin, they owned lower IC_{50} values than that of cisplatin, the IC_{50} values of complexes **I** and **II** against BEL-7404 cells were 11.85 ± 0.06 and 8.40 ± 0.07 μM, respectively, which were approximately one-third of the cisplatin (24.87 ± 0.29 μM). Meanwhile, compared with complex **I**, complex **II** showed stronger cytotoxicity. Such observed different effects of anti-proliferation can be due to the influence of the electronic effect of the methyl group of MeQ in complex **II** [27]. Moreover, complex **II** displayed lower cytotoxic activities to HL-7702 (normal cell), which suggested complex **II** exhibited certain selectivity towards the tested tumor cell lines.

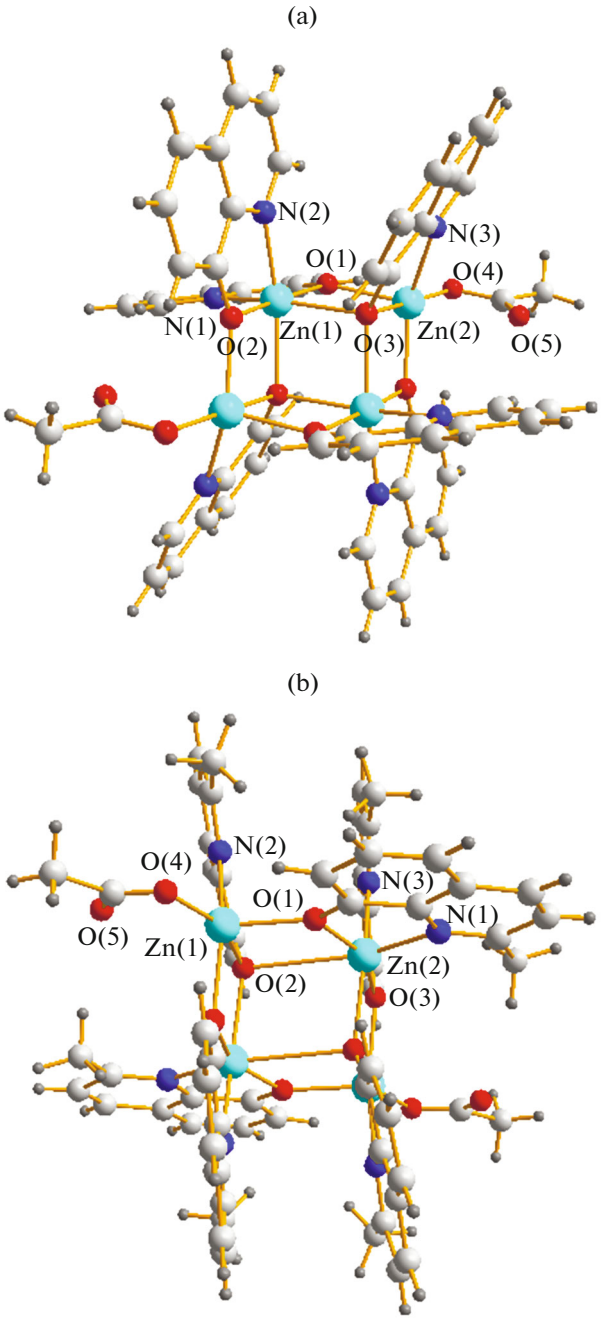

Fig. 1. X-ray crystal structures of complex **I** (a) and **II** (b).

Considering both complexes **I** and **II** exhibited the most sensitive growth inhibition on BEL-7404 cell line, the effects of the two complexes on cell cycle progression of BEL-7404 cell line were investigated using flow cytometry in PI-stained cells. As shown in Fig. 3, BEL-7404 cells incubated with complex **I** at different concentrations (0, 5.0, 10.0, and 15.0 μM) for 48 h showed that S phase populations reduced, while G1 phase populations increased, the respective G1 phase populations were 70.70, 74.51 and 75.23%. Compared with the G1 population of 57.00% for the control cells, they were 13.7, 17.51 and 18.23% higher than that of the control cells, respectively. The results suggested that complex **I** could block cell cycle through G1 phase in a dose-dependent manner. However, BEL-7404 cells treated with different concentrations of complex **II** for 48 h showed that the cell proportion of S phase markedly increased (30.47, 44.05, 61.80 for complex **II** and 23.31% for control), while a dramatic decrease in G1 phase was observed compared with the control cells. These results showed that complex **II** could impede cell cycle through S phase in a dose-dependent manner. The different cell cycle arrest for complexes **I** and **II** may be related to the different HOQ and MeQ structures.

Since cell cycle arrest plays a essential role in the tumor cells apoptosis [28, 29], further evaluations of apoptosis for BEL-7404 cells caused by complexes **I** and **II** were investigated using Annexin V (for the investigation of the characteristic phosphatidylserine residues from the inner cell membrane to outside in the early stage of apoptosis translocated) and PI (for the membrane permeation in necrotic cells) double staining by flow cytometry [30, 31]. As shown in Fig. 4, comparing with the control, the populations of apoptosis cells (including late apoptotic cells in Q2 and early apoptotic cells in Q3) by complexes **I** and **II** were both significantly increased. With the raise of complex **I**, the percentages were increased from 5.3 to 18.7, 23.2, 50.0%, respectively. And with the raise of complex **II**, the percentages were increased from 5.8 to 67.2, 83.0, 92.1%, respectively. The results clearly indicated that complexes **I** and **II** effectively induced apoptosis in BEL-7404 cells in a dose-dependent manner.

Apoptosis is one of the main types of programmed cell death, involving a series of biochemical events leading to specific cell morphology characteristics for example cell shrinkage, nuclear fragmentation, chromatin condensation, and chromosomal DNA fragmentation [32, 33]. The morphology characteristics of the apoptotic BEL-7404 cells were detected by Hoechst 33258 staining. As indicated in Fig. 5, in the control groups, the cell nucleus was dim blue, and the nucleus compared full, while in zebularine treatment groups, nuclear shrinkage, bright chromatin condensation and nuclear fragmentation could be gradually found with treating increasing concentrations of complexes **I** and **II**. The results further revealed that complexes **I** and **II** can induce apoptosis of BEL-7404 cells in a dose-dependent manner [34].

The BEL-7404 cell apoptosis was also examined with AO/EB staining. As observed in Fig. 6, the the live cells of control showed green fluorescence, whereas the apoptotic cells treated with complexes **I** and **II**, the nuclear chromatin of early apoptotic presented bright green-yellow, the nuclear chromatin of late apoptotic cells showed orange-red fluorescence [35, 36]. The higher concentration of complexes, the

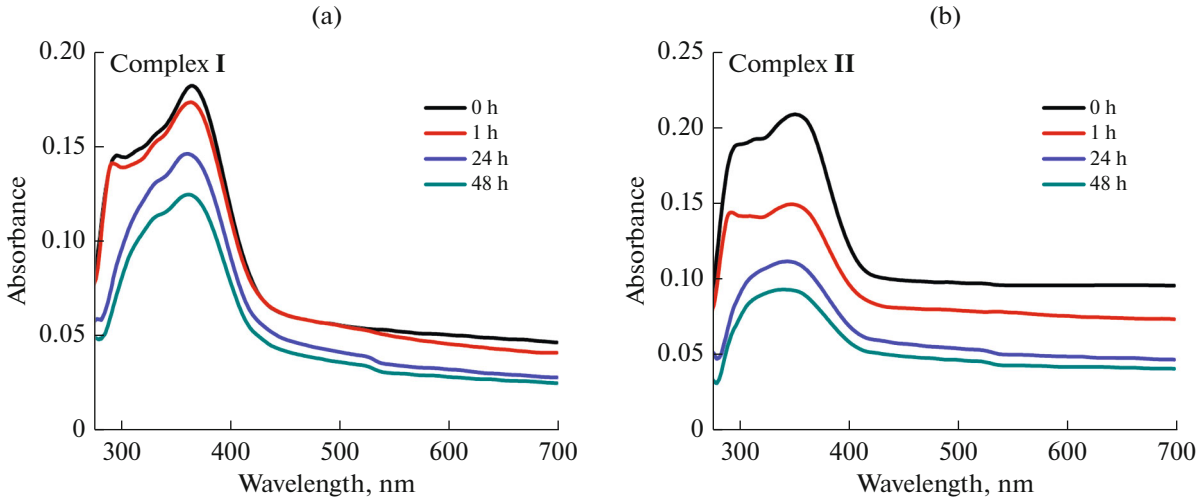

Fig. 2. UV-Vis absorption spectra of complexes **I** (a) and **II** (b) in TSB (2.0×10^{-5} M, containing 1% DMSO) in the time course 0, 1, 24 and 48 h, respectively.

more cells of apoptosis. Those observed results further confirmed that complexes **I** and **II** can induce BEL-7404 cells to produce apoptosis in a dose-dependent manner, and it was consistent with the Hoechst 33258 staining assay.

To explore whether complexes **I** and **II** induced apoptosis was mediated through the intrinsic apoptotic pathway, the changes of mitochondrial membrane potential in BEL-7404 cells were detected by staining Rh 123 using flow cytometry [37]. Rh 123 is a fluorescent dye and its lipophilic cation accumulates inside mitochondria in proportion to its membrane potential. It binds to the inner and outer sides of the inner mitochondrial membrane, as a result, the dye is accumulated by mitochondria in a greater quantity and released upon membrane depolarization [38, 39]. As shown in Fig. 7, right marker showed mitochondria with high membrane potential, i.e., polarized mitochondria, and left marker showed mitochondria with low membrane potential, i.e., depolarized mitochondria. As an effect of complexes **I** and **II**, mitochondrial polarization decreased to 34.3 and 2.1% as compared to control (51.1%), respectively. The results demonstrated that collapse of mitochondrial membrane potential in BEL-7404 cells happened after treated with 10.0 μM complexes **I** and **II**, which implied that the cell apoptosis induced by complexes **I** and **II** might be processed through the intrinsic mitochondrial pathway [40].

Over-expression of intracellular ROS (ROS is reactive oxygen species) is a main cause of leading to DNA and protein damage in apoptotic cells. ROS plays an important role in metabolism, oxidative stress, signal transduction, and apoptosis in cells [41]. The accumulation of intracellular ROS can directly activate the mitochondrial permeability transition and result in loss of mitochondrial membrane potential and the membrane integrity [42, 43]. So generation of ROS is related to cell apoptosis. To investigate effect of ROS generation on apoptosis, BEL-7404 cells were treated with 10.0 μM complexes **I** and **II** for 8 h, respectively, and measured using the stain of DCFH-DA by flow cytometry. As shown in Fig. 8, the treatment cells exhibited high level of ROS (73.2% for complex **I** and 83.0% for complex **II**). Comparatively, the control cells exhibited lower level of ROS (49.6%). These data confirmed that complexes **I** and **II** treatment led to an increase in ROS production. It also suggested that ROS exerted effects on the mitochondria, promoted the decline of mitochondrial membrane potential, and eventually caused cell apoptosis.

Since ROS have a strong relationship with intracellular calcium levels [44], it can alter Ca^{2+} signalling

Table 3. IC_{50} (μM) values of complexes **I** and **II** against six selected tumor cell lines and the normal human liver cell HL-7702 after incubation for 48 h*

Compound	SK-OV-3	BEL-7404	HepG2	HeLa	T-24	MGC-803	HL-7702
I	28.91 ± 0.08	11.85 ± 0.06	13.47 ± 0.07	20.08 ± 0.06	15.80 ± 0.07	12.06 ± 0.04	35.81 ± 0.05
II	43.63 ± 0.05	8.40 ± 0.07	17.68 ± 0.05	11.97 ± 0.05	27.53 ± 0.06	17.96 ± 0.04	50.59 ± 0.07
Cisplatin	4.50 ± 0.06	24.87 ± 0.29	10.34 ± 0.11	1.78 ± 0.08	15.93 ± 0.06	4.19 ± 0.05	4.93 ± 0.06

* IC_{50} values are presented as the mean SD (standard error of the mean) from five separate experiments.

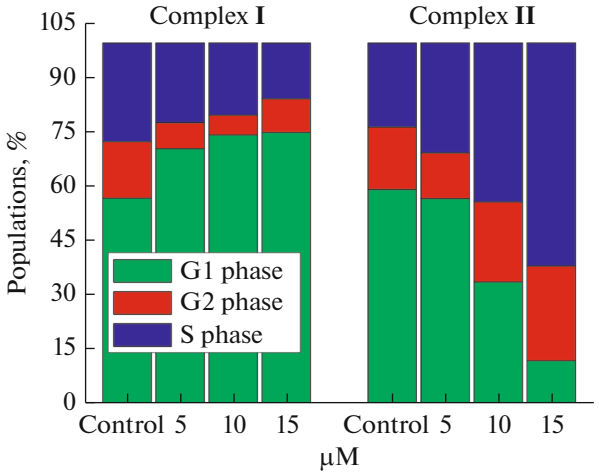

Fig. 3. Cell cycle distribution of BEL-7404 cells after treatment for 48 h with 5.0, 10.0, 15.0 μM of complexes **I** and **II**. Data on each sample represent the percentages of G1, G2, and S.

[45]. And elevated level of intracellular Ca^{2+} is one of the major contributing factors towards the changes in $\Delta\Psi$ [46]. To further ascertain its potentiality in decline of mitochondrial membrane potential and inducing cell apoptosis. The levels of $[Ca^{2+}]_c$ in BEL-7404 cells were monitored by flow cytometry using fluorescent probe Fluo-3/AM. Figure 9 depicted the intracellular calcium levels in BEL-7404 cells treated and untreated with 10.0 μM complexes **I** and **II**. Comparing with the control, BEL-7404 cells exposed to complexes **I** and **II** for 8 h displayed great elevations of $[Ca^{2+}]_c$. The levels of intracellular Ca^{2+} were increased from 49.2 to 80.2, 97.5% after treatment complexes **I** and **II**, respectively. The results indicated that the treatment of complexes **I** and **II** can induce an increase in Ca^{2+} production, which may further lead to decline of mitochondrial membrane potential in BEL-7404 cells apoptosis. It was consistent with the ROS generation assay.

Mitochondrial pro-apoptotic effectors induce massive activation of caspases that in turn activate a proteolytic cascade leading to degradation of cellular components [47]. The mitochondrial intrinsic pathway of apoptosis is regulated by members of the caspase family. The apoptotic process could be confirmed by the presence of caspase-3 and caspase-9 (caspase-3/9), which play an essential role as an executor of apoptosis [22]. To further prove that the cell apoptosis was passed through the intrinsic mitochondrion-mediated apoptotic pathway of complexes **I** and **II**, flow cytometry was adopted to examine the activation of caspase-3/9, in BEL7494 cells after treatment with 10.0 μM complexes **I** and **II** for 8 h with FITC-DEVD-FMK (for caspase-3) and FITC-LEHD-FMK (for caspase-9) probes. As demonstrated in Fig. 10, the expression of activated caspase-3/9 cells were observed remarkable increase in complexes **I** and **II** treated cells compared with the control. The proportions of activated caspase-3 cells treated with com-

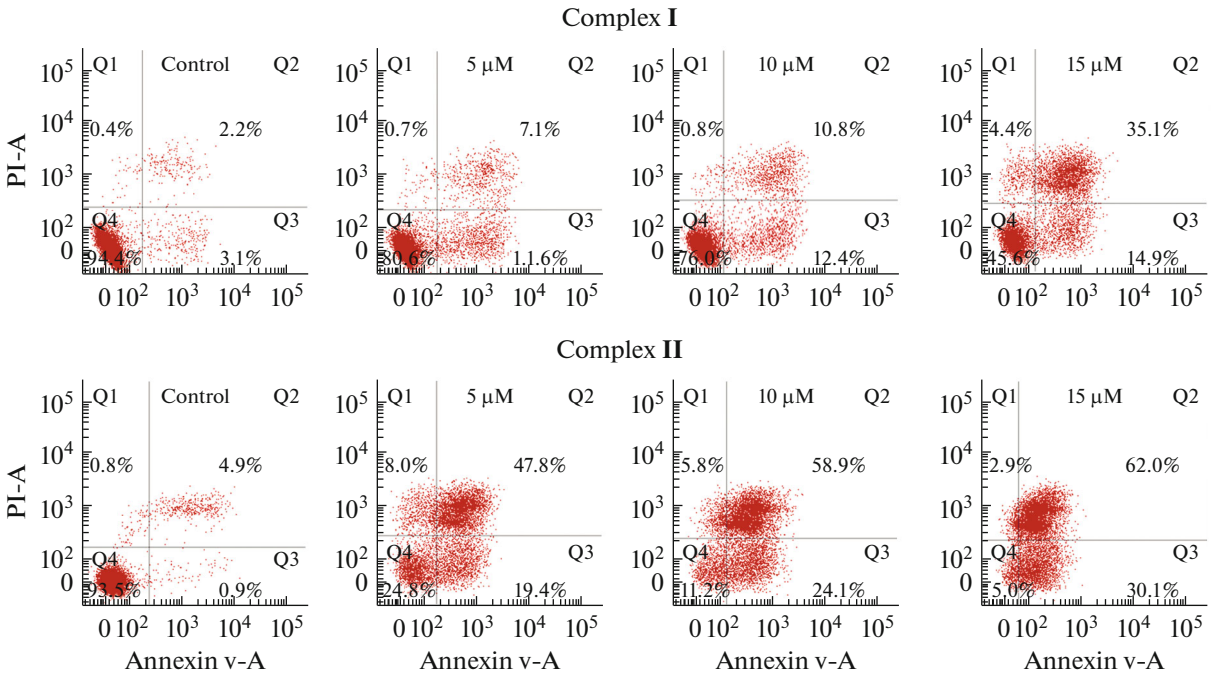

Fig. 4. The induction of apoptosis of BEL-7404 cells treated by complexes **I** and **II** measured by flow cytometry with PI and FITC-Annexin V staining at different concentrations of complexes (5.0, 10.0, and 15.0 μM) for 8 h.

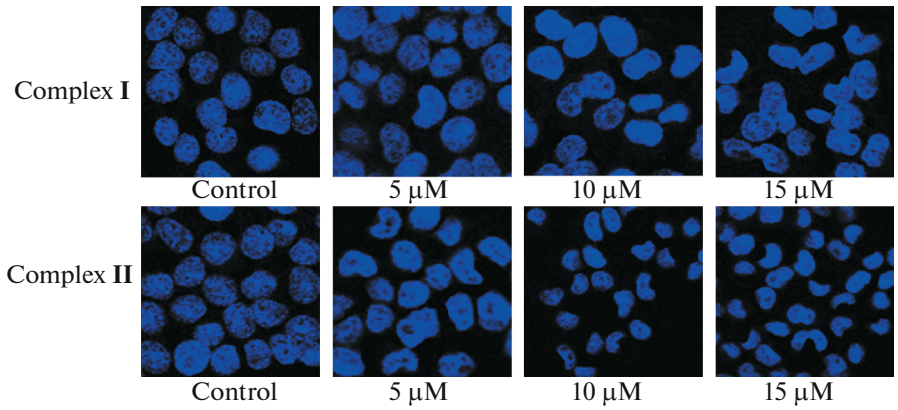

Fig. 5. Apoptosis and morphological changes of BEL-7404 cells induced by the complexes **I** and **II** with various concentrations (5.0, 10.0, and 15.0 μM) for 8 h, and stained by Hoechst 33258.

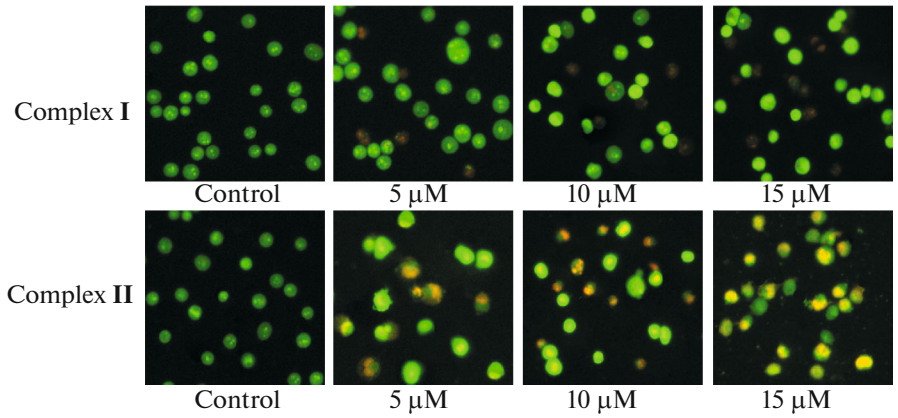

Fig. 6. Apoptosis observation of BEL-7404 cells treated by 5.0, 10.0, and 15.0 μM of complexes **I** and **II** for 8 h, respectively, and stained by AO/EB.

plexes **I** and **II** were 6.2 and 88.5% of total cells, respectively. Meanwhile, the proportions of activated caspase-9 cells exposed to complexes **I** and **II** were 15.1 and 84.5% of total cells, respectively. These results indicated that the cell apoptosis induced by complexes **I** and **II** was through triggering caspase-3/9 activity in BEL-7404 cells by mitochondrion-mediated apoptotic pathway.

DNA is generally accepted as the primary target for anticancer agents. The DNA replication in tumor cells can be blocked by the intercalations between the small molecule and the base pairs of DNA [48]. In an

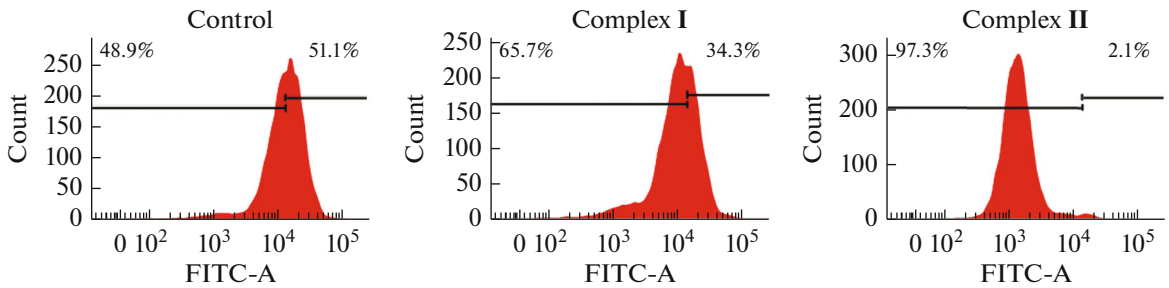

Fig. 7. Collapse of mitochondrial membrane potential in BEL-7404 cells by treated with 10.0 μM complexes **I** and **II** for 8 h using flow cytometry with Rh 123 staining.

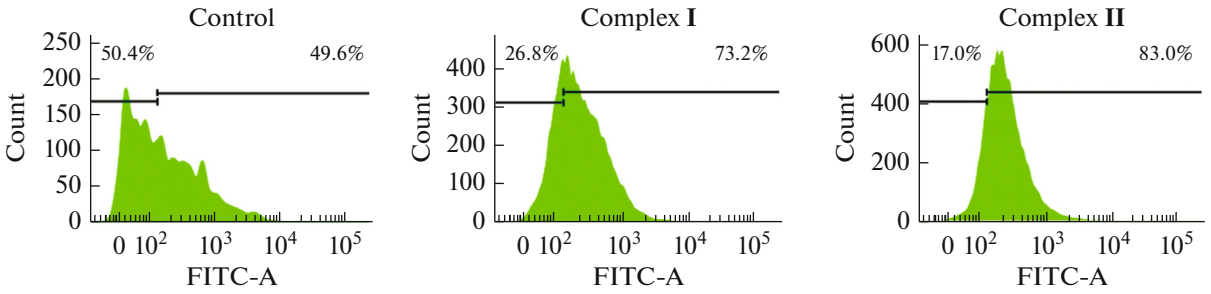

Fig. 8. The generation of ROS by complexes **I** and **II** in BEL-7404 cells treated with 10.0 μM for 8 h.

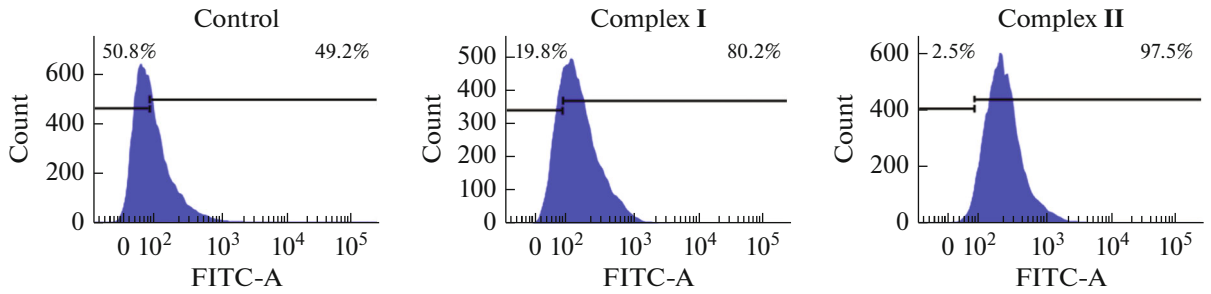

Fig. 9. The level of intracellular Ca^{2+} concentration by complexes **I** and **II** in BEL-7404 cells treated with 10.0 μM for 8 h.

attempt to seek for the potential anti-tumor target of complexes **I** and **II**, DNA binding properties were studied by UV-Vis absorption, CD spectra and agarose gel electrophoresis.

In this work, the electrostatic interactions between **I** and **II** with DNA were considered. SDS was selected as a probe to investigate the electrostatic interaction because of the aggregated dodecyl sulfate anions acting as appropriate substitute for DNA polyanionic backbone, which led to spectral changes that could be detected by UV-Vis absorption spectroscopy [49]. The UV-Vis absorbance of complex **I** changed rarely with the adding of SDS, which indicated that there were weak electrostatic interaction between complex **I** and

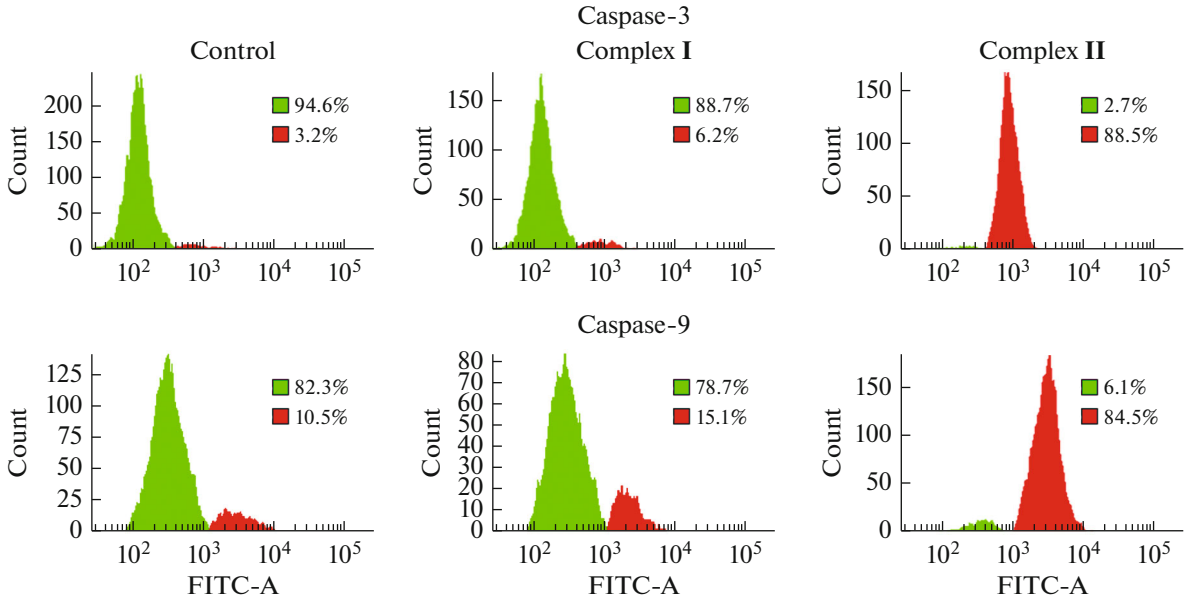

Fig. 10. The activation of caspase-3/9 by complexes **I** and **II** in BEL-7404 cells treated with 10.0 μM for 8 h.

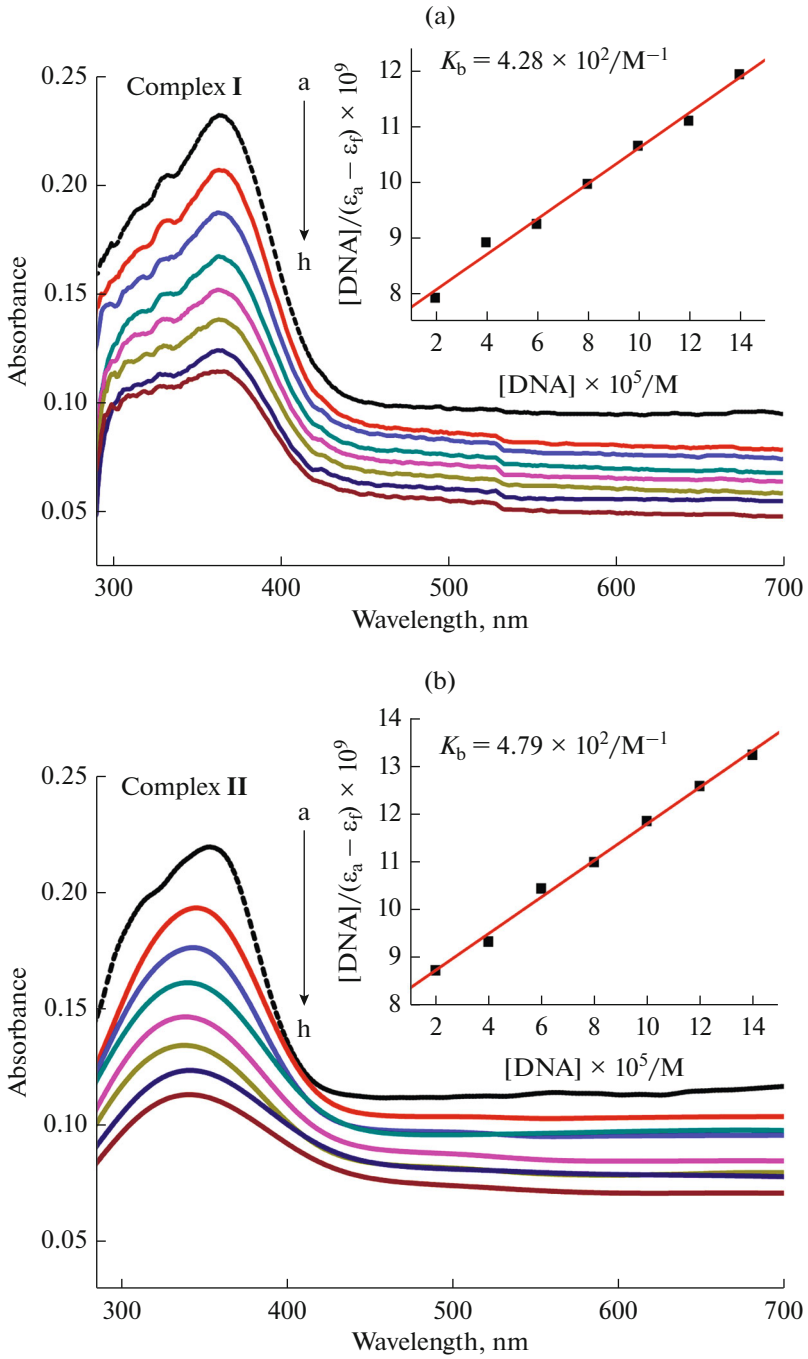

Fig. 11. Absorption spectra of complexes **I** (a) and **II** (b) (2.0×10^{-5} mol/L) in the absence (dashed line) and presence (solid line) of increasing amounts of ct-DNA from 1 : 1 to 7 : 1.

SDS. While the UV-Vis absorption of complex **II** almost not changed, which suggested that the electrostatic interaction between complex **II** and DNA was not existed[2].

In order to further ascertain the possible binding mode between drug and DNA, the interactions of complexes **I** and **II** with ct-DNA had been investigated by UV-Vis absorption titration assay. The extent of hypochromism is commonly consistent with the strength of intercalative interaction [50]. As shown in Fig. 11, there were obvious hypochromic effect on both of complex **I**–DNA system and complex **II**–DNA system with the increasing [complex]/[DNA] ratio from 1 : 1 to 7 : 1. The hypochromic rates of complexes **I** and **II** were 49.2 and 51.7%, respectively. The

[2] Additional material can be gotten from the authors.

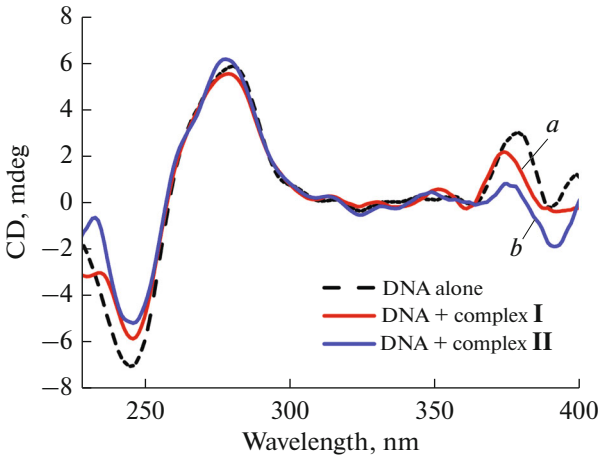

Fig. 12. CD spectra of ct-DNA in the absence (dashed line) and presence (solid line) of the complexes **I** (*a*) and **II** (*b*), [DNA] = 1.0×10^{-4} mol/L, [complex] = 0 and 4.0×10^{-4} mol/L.

K_b values were found to be 4.28×10^2 and 4.79×10^2 M^{-1} corresponding to the complexes **I** and **II**. The characteristic hypochromicity suggested that the complexes **I** and **II** bind intercalatively between the neighboring base pairs of the ct-DNA [51]. Therefore, the most probable binding mode of both complexes **I** and **II** to ct-DNA should be the intercalative binding through the aromatic planar structure of quinoline [52]. The binding constants K_b indicated stronger interaction between complex **II** and ct-DNA than **I**.

To further verify the existing of intercalative binding to ct-DNA, CD spectrum was used to monitor the conformation of ct-DNA in solution. The CD spectrum of ct-DNA exhibits a positive peak at 278 nm because of base stacking and a negative peak at 246 nm because of the helicity of B-type DNA [53]. As shown in Fig. 12, in the presence of complexes **I** and **II**, the negative (~245 nm) peaks greatly increased in absorption, while the positive (~279 nm) peaks had not obvious change. The decrement ratios of the negative peak absorbance were 16.6 and 26.8% for complexes **I** and **II**, respectively. The observed results could be regarded as one of the proofs for their intercalative binding to ct-DNA via the planar aromatic structure of quinolinol [54].

The binding mode of complexes **I** and **II** with pBR322 plasmid DNA was further investigated by agarose gel electrophoresis assay. The pBR322 DNA alone exhibits three forms of DNA with different electrophoretic mobility, containing supercoiled DNA (Form I), nicked DNA (Form II) and linear DNA (Form III). When small molecule of drug interacts with DNA in an intercalation mode, the migration rate of supercoiled DNA decreases [55]. As shown in Fig. 13, the migration rate of Form I gradually reduced and brightness intensity of Form I also gradually decreased with the increasing concentrations of complexes **I** and **II**. Comparing with complex **I**, the migration rate of complex **II** decreased much more under the same concentration. The results revealed that complexes **I** and **II** can bind with DNA by intercalative binding mode. In summary, based on the above different spectral analyses, the main binding mode of complexes **I** and **II** with DNA was intercalation.

The two new 8-hydroxylquinoline-zinc(II) complexes **I** and **II** were synthesized by the reaction of zinc(II) salts with the corresponding quinoline ligands. They were characterized by ESI-MS, elemental analyses, and IR as well as X-ray single crystal diffraction analysis. The two complexes' biochemical effect on human tumor cells and its binding model with DNA were investigated. The complexes **I** and **II** exhibited considerable antitumor activity by inducing apoptosis and causing cell cycle arrest in G1 and S phase, respectively. Complex **II** had higher antitumor activities than complex **I** against BEL-7404 cells. The results from various in vitro assays indicated that both the complexes caused cell apoptosis via eliciting ROS, elevating level of intracellular Ca^{2+} and triggering caspase-3/9 activity mediated by a mitochondrial dysfunction pathway on BEL-7404 cells. The binding properties of complexes **I** and **II** to DNA examined by various methods indicated that intercalation was the most probable binding mode for both the complexes **I** and **II**.

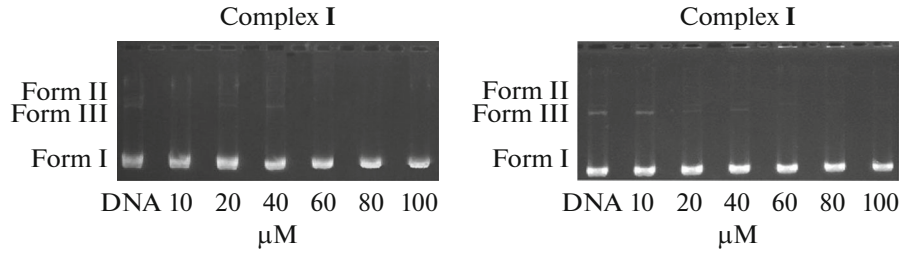

Fig. 13. Gel electrophoresis mobility shift assay of pBR322 DNA treated with increasing concentrations of 10, 20, 40, 60, 80, and 100 μM complexes **I** and **II** at 25°C after 2 h of incubation in TBE buffer.

ACKNOWLEDGMENTS

This work was supported by Scientific Research Project of Hunan Provincial Education Department of China (no. 17C0817) and the Foundation of Key Laboratory for Chemistry and Molecular Engineering of Medicinal Resources (Guangxi Normal University) (CMEMR2016-B14).

REFERENCES

1. Angshuman, R., Dipsikha, B., and Sumanta, K.S., *Dalton Trans.*, 2016, vol. 45, p. 2963.
2. Wei, Q.L., Soo, Z.F.P., Hesheng, V.X., et al., *Nanoscale*, 2016, vol. 8, p. 12510.
3. Gresley, A.L., Gudivaka, V., Carrington, S., et al., *Org. Biomol. Chem.*, 2016, vol. 14, p. 3069.
4. Bravo, I., Alonso-Moreno, C., Posadas, I., et al., *RSC Adv.*, 2016, vol. 6, p. 8267.
5. Wahab, R., Khan, F., Yang, Y.B., et al., *RSC Adv.*, 2016, vol. 6, p. 26111.
6. Kljun, J., Anko, M., Traven, K., et al., *Dalton Trans.*, 2016, vol. 45, p. 11791.
7. Rosenberg, B., van Camp, L., Trosko, J.E., et al., *Nature*, 1969, vol. 222, p. 385.
8. Sultana, K., Zaib, S., Khan, N.H., et al., *New J. Chem.*, 2016, vol. 40, p. 7084.
9. Ni, L., Wang, J., Liu, C., et al., *Inorg. Chem. Front.*, 2016, vol. 3, p. 959.
10. Kljun, J., Anko, M., Traven, K., et al., *Dalton Trans.*, 2016, vol. 45, p. 11791.
11. Frederickson, C.J., Koh, J.Y., and Bush, A.I., *Nat. Rev. Neurosci.*, 2005, vol. 6, p. 449.
12. König, S.G., Öz, S., and Krämer, R., *Mol. BioSyst.*, 2016, vol. 12, p. 1114.
13. Ghosh, K., Kumar, P., and Tyagi, N., *Inorg. Chim. Acta*, 2011, vol. 375, p. 77.
14. Shiri, F., Shahraki, S., Baneshi, S., et al., *RSC Adv.*, 2016, vol. 6, p. 106516.
15. Freitas, L.B.D.O., Borgati, T.F., Freitas, R.P.D., et al., *Eur. J. Med. Chem.*, 2014, vol. 84, p. 595.
16. Liu, Y.C. and Yang, Z.Y., *J. Org. Chem.*, 2009, vol. 694, p. 3091.
17. Lam, K.H., Gambari, R., Lee, K.K.H., et al., *Bioorg. Med. Chem. Lett.*, 2014, vol. 24, p. 367.
18. Chan, A.S.C., Tang, J.C.O., Lam, K.H., et al., US Patent 0054482, 2009.
19. Chan, S.H., Chui, C.H., Chan, S.W., et al., *ACS Med. Chem. Lett.*, 2013, vol. 4, p. 170.
20. Sheldrick, G.M., *SHELXS-97, Program for the Solution of Crystal Structures*, Göttingen: Univ. of Göttingen, 1997.
21. Lu, J., Sun, Q., Li, J.L., et al., *J. Inorg. Biochem.*, 2014, vol. 137, p. 46.
22. Qin, Q.P., Chen, Z.F., Shen, W.Y., et al., *Eur. J. Med. Chem.*, 2015, vol. 89, p. 77.
23. Bishayee, K., Chakraborty, D., Ghosh, S., et al., *Eur. J. Pharm.*, 2013, vol. 698, p. 110.
24. Zainal, A.S.H., Wan, O.W.H., Zainal, A.Z., et al., *Cancer Cell Int.*, 2009, vol. 9, p. 1.
25. Sattarzadeh, E., Mohammadnezhad, G., Amini, M.M., et al., *Acta Crystallogr., Sect. E*: *Struct. Rep.* Online, 2009, vol. 65, no. 7, p. 712.
26. Arjmand, F., Yousuf, I., Afzal, M.L., et al., *Inorg. Chim. Acta*, 2014, vol. 421, p. 26.
27. Madonna, S., Marcowycz, A., Lamoralptheys, D., et al., *J. Heterocycl. Chem.*, 2010, vol. 47, p. 719.
28. Long, F., Dong, C.Y., Jiang, K.Q., et al., *RSC Adv.*, 2017, vol. 7, p. 21342.
29. Chou, C.C., Yang, J.S., Lu, H.S., et al., *Arch. Pharm. Res.*, 2010, vol. 33, p. 1181.
30. Romero-Canelón, I., Salassa, L., and Sadler, P.J., *J. Med. Chem.*, 2013, vol. 56, p. 1291.
31. Ma, Z.Y., Qiao, X., Xie, C.Z., et al., *J. Inorg. Biochem.*, 2012, vol. 117, p. 1.
32. Qiu, R., Chen, J., Sima, J., et al., *J. Cancer Res. Clin. Oncol.*, 2012, vol. 138, p. 119.
33. Tan, W., Zhou, W., Yu, H.G., et al., *Biochem. Biophys. Res. Commun.,* 2013, vol. 430, p. 250.
34. Ouyang, M., Zeng, L.L., Huang, H.Y., et al., *Dalton Trans.*, 2017, vol. 46, p. 6734.
35. Subramaniyan, B., Kumar, V., and Mathan, G., *Biomed. Pharmacother.*, 2017, vol. 90, p. 402.
36. Liu, Z.G., Xiang, Q.S., Du, L.H., et al., *Food Chem.*, 2013, vol. 141, p. 289.
37. Cunha-Oliveira, T., Rego, A.C., Cardoso, S.M., et al., *Brain Res.*, 2006, vol. 1089, p. 44.
38. Singh, B.K., Tripathi, M., Pandey, P.K., et al., *Toxicol.*, 2010, vol. 275, p. 1.
39. Zamzami, N., Maisse, C., Metivier, D., et al., *Methods Cell Biol.*, 2007, vol. 80, p. 327.
40. Musa, M.A., Latinwo, L.M., Virgile, C., et al., *Bioorg. Chem.*, 2015, vol. 58, p. 96.
41. Apel, K.H., *Annu. Rev. Plant Biol.*, 2004, vol. 55, p. 373.
42. Crompton, M., Barksby, E., Johnson, N., et al., *Biochimie*, 2002, vol. 84, p. 143.
43. Ma, W.D., Zou, Y.P., Wang, P., et al., *Food Chem. Toxicol.*, 2014, vol. 70, p. 1.
44. Pachauri, V., Mehta, A., Mishra, D., et al., *Neurotoxicology*, 2013, vol. 35, p. 137.
45. Girish, K.S., Paul, M., Thushara, R.M., et al., *Biochem. Biophys. Res. Commun.*, 2013, vol. 438, p. 198.
46. Leytin, V., *Blood, Rev.*, 2012, vol. 26, p. 51.
47. Martins, C., Doran, C., Silva, I.C., et al., *Chem. Biol. Interact.*, 2014, vol. 218, p. 1.
48. Dutta, S., Abe, H., Aoyagi, S., et al., *J. Am. Chem. Soc.*, 2005, vol. 127, p. 15004.
49. Ma, D.L. and Che, C.M., *Chem. Eur. J.*, 2003, vol. 9, p. 6133.
50. Krishnamoorthy, P., Sathyadevi, P., Butorac, R.R., et al., *Dalton Trans.*, 2012, vol. 41, p. 4423.
51. Galindo, M.A., Olea, D., Romero, M.A., et al., *Chem. Eur. J.*, 2007, vol. 13, p. 5075.
52. Ihmels, H. and Otto, D., *Top. Curr. Chem.*, 2005, vol. 258, p. 161.
53. Li, P., Niu, M.J., and Hong, M., *J. Inorg. Biochem.*, 2014, vol. 137, p. 101.
54. Xu, H., Zheng, K.C., Chen, Y., et al., *Dalton Trans.*, 2003, vol. 2003, p. 2260.
55. Dunham, S.U., Chifotides, H.T., Mikulski, S., et al., *Biochemistry*, 2005, vol. 44, p. 996.